IOP Publishing Plasma Sources Science and Technology
Plasma Sources Sci. Technol. 26 (2017) 025005 (13pp) doi:10.1088/1361-6595/aa5300

Characterization of inductively coupled plasma generated by a quadruple antenna

G Shafir[1], D Zolotukhin[2], V Godyak[3], A Shlapakovski[1], S Gleizer[1], Ya Slutsker[1], R Gad[1], V Bernshtam[4], Yu Ralchenko[5] and Ya E Krasik[1]

[1] Physics Department, Technion, Haifa 36000, Israel
[2] Physics Department, Tomsk State University of Control Systems and Radioelectronics, Tomsk 634050, Russia
[3] Electrical Engineering and Computer Science Department, University of Michigan, Ann Arbor, MI 48109, USA
[4] Faculty of Physics, Weizmann Institute of Science, Rehovot 36100, Israel
[5] National Institute of Standards and Technology, Gaithersburg, MD 20899-8422, USA

E-mail: shafirguy@gmail.com

Received 12 August 2016, revised 11 November 2016
Accepted for publication 9 December 2016
Published 17 January 2017

Abstract

The results of the characterization of large-scale RF plasma for studying nonlinear interaction with a high-power (~400 MW) short duration (~0.8 ns) microwave (~10 GHz) beam are presented. The plasma was generated inside a Pyrex tube 80 cm in length and 25 cm in diameter filled by either Ar or He gas at a pressure in the range 1.3–13 Pa using a 2 MHz RF generator with a matching system and a quadruple antenna. Good matching was obtained between the plasma parameters, which were determined using different methods including a movable Langmuir probe, microwave cut-off, interferometry, and optical emission spectroscopy. It was shown that, depending on the gas pressure and RF power delivered to the antenna, the plasma density and electron temperature can be controlled in the range 1×10^{10}–5×10^{12} cm^{-3} and 1–3.5 eV, respectively. The plasma density was found to be uniform in terms of axial (~60 cm) and radial (~10 cm) dimensions. Further, it was also shown that the application of the quadruple antenna, with resonating capacitors inserted in its arms, decreases the capacitive coupling of the antenna and the plasma as well as the RF power loss along the antenna. These features make this plasma source suitable for microwave plasma wake field experiments.

Keywords: RF plasma, inductive coupling, Langmuir probe diagnostics, microwave interferometry, spectroscopy

(Some figures may appear in colour only in the online journal)

1. Introduction

The research of the wake fields formed in high density (10^{17}–10^{18} cm^{-3}) plasma by a powerful (>10^{18} W cm^{-2}) laser pulse with duration 10^{-14}–10^{-15} s is of increasing interest worldwide because of the extremely high electric fields (10^{8}–10^{9} V cm^{-1}) generated in the plasma [1–3]. This electric field can be efficiently used for electron/ion acceleration to relativistic energies within a length scale of $\leqslant 10^{-2}$ m.

To study the wake-field formation resulting from plasma density modulation, we suggest using a short duration (<1 ns) powerful (>400 MW) microwave (10 GHz) beam. Such studies require that a cylindrical plasma column with the following parameters be generated:

(a) The radius and length of the plasma column are larger than those of the beam.
(b) The plasma density is uniform in radial and axial dimensions.
(c) The electron plasma frequency is lower than that of the microwave.
(d) The plasma is generated without using immersed electrodes.
(e) The experimental setup allows plasma diagnostics with electrical probes and microwave and optical methods.

When applying these requirements in the case of a 0.5 ns pulse duration (length of ~15 cm) microwave beam with a frequency of 10 GHz, plasma with electron density, n_e, in the range of $(10^{10}$–$10^{12})\,cm^{-3}$ and having a diameter of ~20 cm and a length of ~60 cm is required. Different methods can be applied to generate this type of the plasma. For instance, large-scale uniform plasma can be generated using helicon excited plasma waves [4]. Such plasma can be formed in meter longitudinal scale with $n_e \leqslant 10^{14}\,cm^{-3}$ in the form of an axially uniform cylindrical column with diameters of tens of cm by applying axial magnetic fields up to several hundreds of Gauss [4, 5]. Windish *et al* [6] demonstrated the formation of Ar plasma with $n_e \sim 10^{10}\,cm^{-3}$ and electron temperature $T_e = (4$–$7)\,eV$ using helicon waves. The plasma was uniform over a meter-long chamber, with a plane spiral coil placed at one end of the dielectric chamber immersed in a magnetic field up to 1000 G. Shinohara *et al* [7, 8] demonstrated the generation of a 480 cm long and 75 cm diameter Ar plasma source with $n_e \sim 10^{12}\,cm^{-3}$. Control of the radial density profile has been achieved by varying the external magnetic field configurations and the antenna field patterns. However, the external magnetic field in the helicon discharge can affect the interaction between the microwave beam and the magnetized plasma electrons [9].

Another method to generate large scale plasma is to apply an electron-beam source with an electron energy of several keV and current up to 0.5 A [10]. These electrons ionize the background gas generating plasma with an electron density up to $10^{12}\,cm^{-3}$. However, to achieve plasma uniformity over a large distance, a guiding magnetic field must be applied in order to overcome electron scattering, and a large diameter electron beam source should also be developed. The same concern applies to ferroelectric plasma sources [11], which can be used for generating plasma that is uniform in the axial direction with a rather broad range of density $(10^{11}$–$10^{14}\,cm^{-3})$. Such plasma, however, is not uniform in the radial direction [12].

Capacitive coupled plasma (CCP) discharges are widely used for generating plasma with $n_e = (10^{9}$–$10^{11})\,cm^{-3}$ inside a chamber using two disc-shaped parallel electrodes [13–15]. However, when the electrodes' area is enlarged, the RF power deposition and plasma density profiles become non-uniform. The latter is related to standing waves and edge effects, which are difficult to avoid when the plasma source employs power coupling elements with a scale length comparable to quarter of the wavelength of the driving RF power [16, 17]. Because of the sheaths that exist between the plasma boundary and the electrodes, high RF power at relatively low RF frequency ($\leqslant$6 MHz) generates a high RF voltage across the sheaths and, respectively, high RF plasma potential. The latter leads to the acceleration of ions and neutrals (via the ion charge exchange process) toward the electrodes causing them to sputter, leading to plasma contamination. Moreover, at low gas pressure and high RF power, a large part of the RF power is transferred to ion acceleration, thus reducing plasma generation efficiency [18]. In addition, a high plasma RF potential makes Langmuir probe diagnostics difficult [19].

An attractive method to produce the plasma for microwave wake field experiments is to use inductively coupled plasma (ICP). ICP is generated by an electric field induced by a coil powered by an RF current [13]. Inductively coupled gas discharge also can generate a relatively uniform plasma in a wide range of densities $(10^{10}$–$10^{13}\,cm^{-3})$ and, contrary to CCP, ICP is able to efficiently generate a high density plasma at low gas pressure [20]. Typical radii and lengths of ICP sources are in the range 2–25 cm and 3–50 cm, respectively, and plasma densities and electron temperatures obtained in such systems (depending on the size of the plasma, gas pressure, and power) are in the range of 10^{10}–$10^{13}\,cm^{-3}$ and 1–10 eV, respectively [21–23]. One of the most frequently used configurations of ICP sources includes a helical antenna wound around a dielectric chamber [14]. However, in order to generate a plasma column $\sim 10^2$ cm in length a large number of turns of the antenna around the chamber is needed, which leads to an undesirable increase in the capacitive coupling. The latter results in an increase in the RF voltage that must be applied to form the plasma, leading to an increase in the plasma RF potential. Kim *et al* [22] used ICP that consisted of a few segments with different RF currents controlled by variable capacitors. An increase in the RF antenna current in the peripheral ICP area resulted in improved plasma radial uniformity, namely, a uniform plasma formation (~2.4%) over a 30 cm diameter was obtained.

For wake field experiments, the plasma density radial and axial distributions should be well defined. Thus, in order to obtain reliable data, different diagnostics methods should be applied in order to verify the data obtained.

An RF-compensated Langmuir probe can be used to measure the radial and axial distributions of the plasma density, electron temperature, and plasma potential. This probe allows one to obtain the electron energy probability function (EEPF) $f_p(\varepsilon) = F(\varepsilon)/\sqrt{\varepsilon}$, where ε is the energy of electron and $F(\varepsilon)$ is the electron energy distribution function (EEDF). Plasma parameters are calculated as corresponding integrals of the measured EEPF [23, 24]. Plasma parameters determined in this way are more accurate than those obtained by the classical Langmuir probe diagnostics that assumes a Maxwellian EEPF [25].

The data obtained by a Langmuir probe can be verified by the microwave cut-off method and by an interferometry method to measure the spatially averaged plasma electron density along a chosen direction in the plasma. The microwave cut-off method is based on the reflection of the electromagnetic wave from the plasma having a plasma electron frequency larger than the microwave frequency. Kim *et al* [26] performed microwave cut-off measurements of large cylindrical (40 cm in diameter) ICP of Argon plasma using immersed antennas and a network analyzer for measuring the spectrum of the transmitted signal, thus determining the electron plasma frequency and, respectively, the plasma density. The microwave interferometry method allows one to measure the electron density in the plasma by measuring the phase shift of microwaves transmitted through the plasma [27]. For example, Andrasch *et al* [28] used a microwave interferometer to determine the

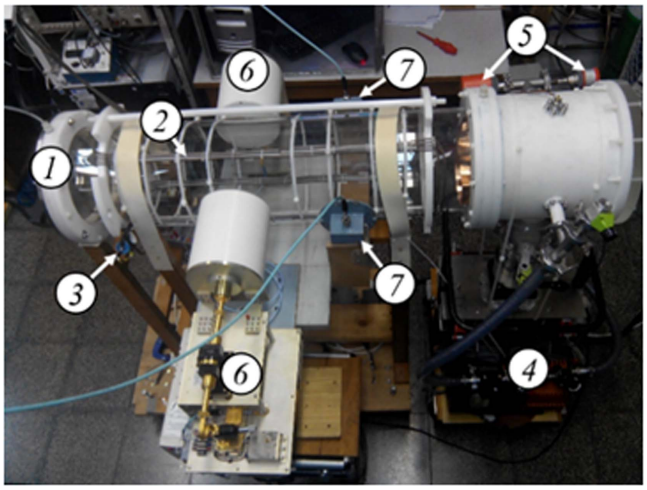

Figure 1. External view of the experimental set-up. (1) Pyrex vacuum chamber; (2) quadruple antenna; (3) resonating capacitors; (4) pumping system; (5) vacuum meter gauges; (6) receiver (up) and transmitter (down) of microwave interferometer; (7) receiver and transmitter for microwave cut-off measurements.

electron density of ICP generated in a cylindrical volume in Ar gas at a pressure range 0.1–10 Pa. For calculating density, the radial density profile, which was determined using a Langmuir probe, was used.

Finally, optical emission spectroscopy (OES) is another non-invasive diagnostics method, which can be used for ICP. For example, Iordanova *et al* [29] used collisional radiative modeling to determine the electron density and electron temperature of low pressure Argon plasma by measuring the ratio between the intensities of different Argon lines, combined with line broadening measurements.

In this paper, we describe a plasma source for a microwave wake field experiment. In order to obtain a long plasma source and to decrease capacitive coupling, we used a 4-turn, symmetrically driven, quadruple antenna located crosswise and stretched along the plasma chamber. The main goals of this research were to generate large scale ICP by using a quadruple antenna and to measure the plasma parameters for different types of gas, pressure, and delivered power. It was shown that the inductively coupled discharge with a quadruple antenna produces rather uniform cylindrical plasma with a length of ~60 cm and diameter of ~20 cm. The plasma parameters were determined using the data obtained by means of different diagnostics, namely, a Langmuir probe, microwave interferometry, microwave cut-off, and OES. Depending on the type and pressure of the gas and the RF power delivered to the antenna, the plasma electron density ranged between 1×10^{10}–5×10^{12} cm^{-3}, with an electron temperature of 1–5 eV. This plasma source meets the requirements for a microwave wake field experiment.

2. Experimental setup and diagnostics

An external view of the experimental setup is shown in figure 1. A 1 m long cylindrical Pyrex tube with an inner

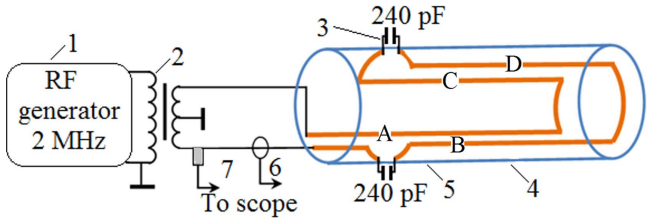

Figure 2. (a) Electrical scheme of the ICP drive. (1). RF generator; (2) step-down balun transformer; (3) resonating capacitors; (4) antenna coil; (5) Pyrex tube; (6) pearson current transformer; (7) RF voltage probe. the terms (a)–(d) represent the four azimuthal directions of the antenna.

diameter of 24 cm was used. A quadruple antenna, 80 cm long, made of insulated Cu wire, 2 mm in diameter, was mounted onto the Pyrex tube. The antenna coil consisted of four quadruple turns with four arms, azimuthally separated by 90^0 from each other.

The tube was preliminarily pumped to a pressure of 4×10^{-3} Pa by a turbo-molecular pump, and then, filled with either Ar or He gas at a continuous flow to a pressure in the range 0.6–13 Pa. The gas input and output ports were located at opposite ends of the Pyrex tube. A sketch and the electrical scheme of the system are shown in figure 2.

The ICP was produced using an RF generator (HFV8000, 2 MHz, and output power $\leqslant$5 kW at matched 50 Ω load). The main application of the HFV8000 RF generator implies its cw operation. In our experiments we used its additional feature allowing externally controlled generator operation in the pulsed mode. However, because of the transition period of ~150 ms duration of the output power and frequency self-adjustment by internal electronic scheme, the RF pulse duration was >200 ms. In order to resonate the antenna having an inductance of $L_a = 53$ μH, two ceramic capacitors (240 pF each) were each connected in series to the antenna. The output of the RF generator was connected to the antenna using a highly efficient transmission line step-down transformer having symmetrical outputs with variable transformer ratio [20].

The plasma was ignited and maintained by the application of a 300 ms duration RF pulse. The antenna voltage (at its input) and current were measured with a 1:1000 voltage probe (Tektronix P6105A) and a Pearson current transformer (Pearson electronics CM-10-M), respectively. The signals from the voltage and current sensors were acquired and processed with a Tektronix TDS784A digital oscilloscope.

The power delivered to the plasma, P_p, and that dissipated in the antenna, P_0, were calculated using the voltage and current measured at the antenna input without plasma, ($V_0(t)$, $I_0(t)$), and with plasma, ($V(t)$, $I(t)$). Then, P_p was determined according to the expressions [20]

$$R_0 = \langle I_0(t) \cdot V_0(t) \rangle / \langle I_0^2(t) \rangle \text{ and}$$
$$P_p = \langle I(t) \cdot V(t) \rangle - \langle I^2(t) \rangle R_0 = P_t - P_0, \quad (1)$$

where P_t is the power transmitted to the antenna loaded with plasma, R_0 is the antenna RF Ohmic resistance without

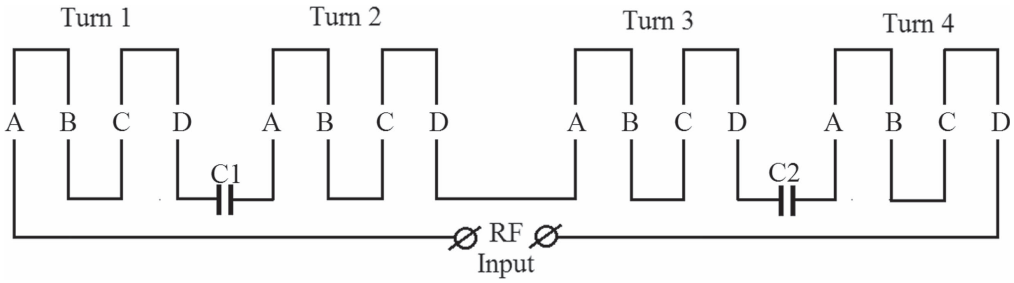

Figure 3. Circuit diagram of the antenna coil with capacitors C1 and C2 inserted between the turns. The terms A–D represent the four azimuthal directions of the antenna.

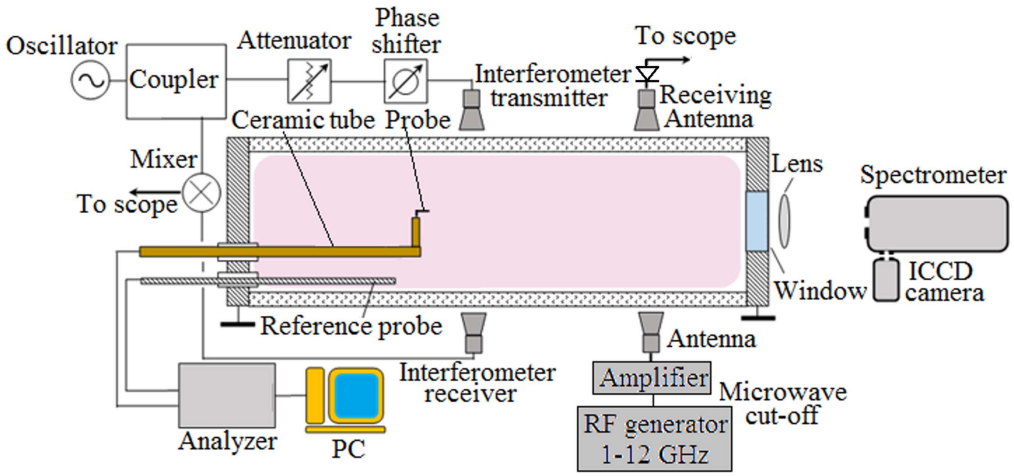

Figure 4. Schematic drawing of the diagnostics used for the ICP research.

plasma, and brackets $\langle\ \rangle$ mean the average over an RF period.

Different locations of the capacitors' connections to the antenna coil were tested; namely, the capacitors were connected either at the both ends of the antenna or were inserted between the antenna turns, as shown in figure 3. In both cases the capacitors' capacitance satisfies the resonance condition $(\omega C)^{-1} = \omega L$, thus decreasing the coil RF potential referenced to ground. However, symmetrical insertion of the capacitors between the coil turns not only decreases the coil RF potential and correspondingly the antenna power loss due to capacitive coupling between the coil and the plasma but also decreases significantly capacitive coupling between the coil turns. Let us note also, that in the case of quadrupole antenna one obtains significantly faster decay of outside electric and magnetic fields than in the case of a dipole antenna application.

For the plasma characterization, four types of diagnostics were used: a movable Langmuir probe, microwave interferometry, microwave cut-off, and OES, as shown in figure 4. The RF compensated Langmuir probe manufactured by plasma sensors [30] was mounted on a long, moveable, and azimuthally rotatable ceramic tube. The Langmuir probe was connected to a multi-functional probe analyzer (MFPA) [30], controlled by a remote PC. For each RF pulse, the analyzer generated and processed 100 probe *I–V* curves, each with a duration of 1.5 ms. The plasma electron density and temperature and the plasma potential were calculated by averaging and processing the measured probe *I–V*. The method of measuring and processing the probe *I–V* is described in detail in [24]. The EEPF was determined using the second derivative of the probe *I–V* characteristic $j_e(V)$ versus the bias voltage V of the Langmuir probe:

$$\frac{\mathrm{d}^2 j_e}{\mathrm{d}V^2} = -\frac{e^2}{4}\sqrt{\frac{2e}{mV}}F(\varepsilon) = \frac{e^3}{2\sqrt{2m}}f_p(\varepsilon). \tag{2}$$

Here, e and m are the charge and mass of the electron, respectively. In the case of a Maxwellian electron energy distribution, one obtains a straight line in a semi-log scale of the EEPF versus the probe bias voltage (electron energy). The plasma potential is at the zero-crossing point of $\mathrm{d}^2 j_e/\mathrm{d}V^2$ and the values of the electron density n_e and the electron temperature, T_e, are defined as [24]:

$$n_e = \int_0^\infty \sqrt{\varepsilon} f_p(\varepsilon)\mathrm{d}\varepsilon = \frac{2\sqrt{2m/e}}{e}\int_0^{-\infty} j_e''(V)\sqrt{V}\mathrm{d}V, \tag{3}$$

$$T_e = \frac{2}{3n_e}\int_0^\infty \varepsilon^{3/2} f_p(\varepsilon)\mathrm{d}\varepsilon = \frac{4\sqrt{2m/e}}{3n_e}\int_0^{-\infty} j_e''(V)V^{3/2}\mathrm{d}V. \tag{4}$$

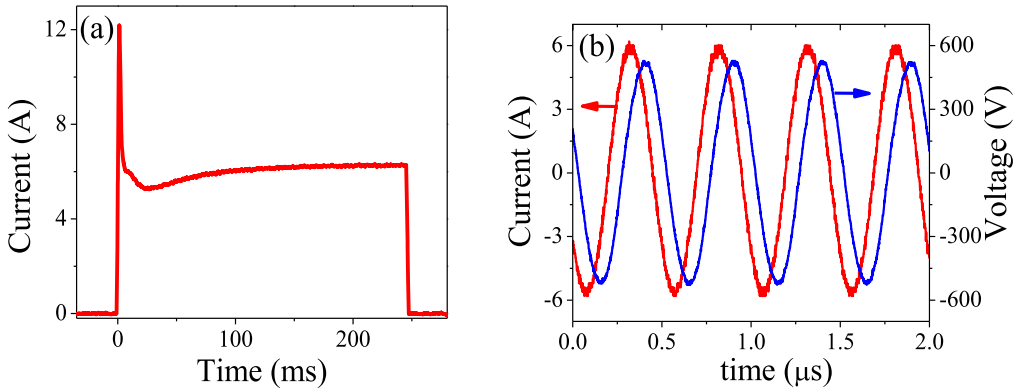

Figure 5. Typical waveforms of (a) the antenna current envelope, measured by the RF diode and (b) instantaneous voltage and current at $t = 150$ ms from plasma ignition. ICP is formed in Ar gas at a pressure of 6.5 Pa and the power delivered to the plasma was 750 W.

The microwave cut-off measurement was performed using a variable frequency RF generator (Agilent model E8257D) operated in continuous wave mode within a frequency range 1–12 GHz. The generator frequency ω was varied until full microwave cut-off at $\omega = \omega_{\text{cutoff}}$ corresponding to the plasma density [31]:

$$n_{\text{e}} = \frac{m_{\text{e}}\varepsilon_0}{\text{e}^2}\omega_{\text{cutoff}}^2. \tag{5}$$

Here, ε_0 is the vacuum permittivity.

A microwave interferometer was used to measure the average plasma density in the radial direction. The interferometer consisted of a 26 GHz Gunn diode oscillator, phase shifter, attenuator, mixer, and transmitting and receiving antennas. One arm of the interferometer was connected to the transmitting antenna via the phase shifter and attenuator. The microwave signal was transmitted through the plasma and sensed by the receiving antenna. The plasma generated in the pulsed mode leads to the appearance of a phase shift in the transmitting electromagnetic waves. The second arm of the interferometer was connected to the mixer, where the microwave signals from the two arms were mixed. The output of the mixer, i.e., the envelope pulse of the two electromagnetic waves, was fed to the digitizing oscilloscope. Before each set of experiments, the attenuator and phase shifter were adjusted to give a zero phase shift without plasma. In this configuration, the phase shift of the electromagnetic wave acquired during the wave propagation in plasma can be defined as [27]:

$$\begin{aligned}\Delta\phi &= \frac{\omega}{c}\int_{-x}^{x}(N(x') - 1)\,\text{d}x' \\ &= \frac{\omega}{c}\int_{-x}^{x}\left(\sqrt{1 - \frac{n_{\text{e}}(x)}{n_{\text{c}}}} - 1\right)\text{d}x',\end{aligned} \tag{6}$$

where N is the index of refraction and $n_{\text{e}}(x)$ is the electron density along the path of the wave. The integral in equation (6) was calculated by fitting the radial profile of the electron density measured by the Langmuir probe for the same experimental conditions.

Another method to measure the average electron temperature and density is spectroscopy. In the conditions of the present experiment with a highly non-equilibrium plasma, the electron density and temperature are too low to allow a local thermodynamic equilibrium (LTE) model of energy level populations. Furthermore, the energy equilibration relaxation times between electrons and ions are hundreds of ms, and therefore, Doppler broadening of excited ions and neutrals cannot be used to measure T_{e}. Thus, in order to determine the plasma density and electron temperature, a time-dependent collisional-radiative (CR) modeling of H and He plasmas was conducted [32]. The density and temperature were determined by comparing the spectral lines intensity ratio obtained by the model to the measured lines ratio. The spectral line intensities were measured by a SPEX 750 M spectrometer equipped with a 2400 grooves mm^{-1} grating and an ICCD 4QuikE camera (Stanford Computer Optics) at its output. A 25 cm focal length lens was used to collect and focus the light emission from the plasma to the entrance slit of the spectrometer. The spectral resolution of the setup of 0.06 A pixel^{-1} was determined using Oriel spectral lamps.

3. Experimental results

3.1. ICP electrical characteristics

The electrical properties of the quadruple antenna without plasma were measured at the different positions of the capacitors in the antenna circuit. We measured the antenna resistance as $R_0 = 10.5\ \Omega$ (corresponding to the unloaded antenna Q-factor $Q_0 = \omega L_{\text{a}}/R_0 = 67$) when the resonating capacitors were placed on the antenna ends, and $R_0 = 3.9\ \Omega$ (corresponding to $Q_0 = 170$) when the capacitors were placed between the antenna turns, as shown in figure 3. The significant difference in the measured values of R_0 and the corresponding power loss in the antenna ($P_0 \propto R_0$) are due to the considerable reduction in the distributed capacitive coupling of the antenna to the Pyrex chamber and plasma when the capacitors were placed between the antenna turns. Further, all measurements were performed with the capacitors inserted.

The electrical parameters of the antenna loaded with plasma were measured in Ar and He gas at pressure ranges 0.8–6.5 Pa and 1.8–13 Pa, respectively. Examples of typical

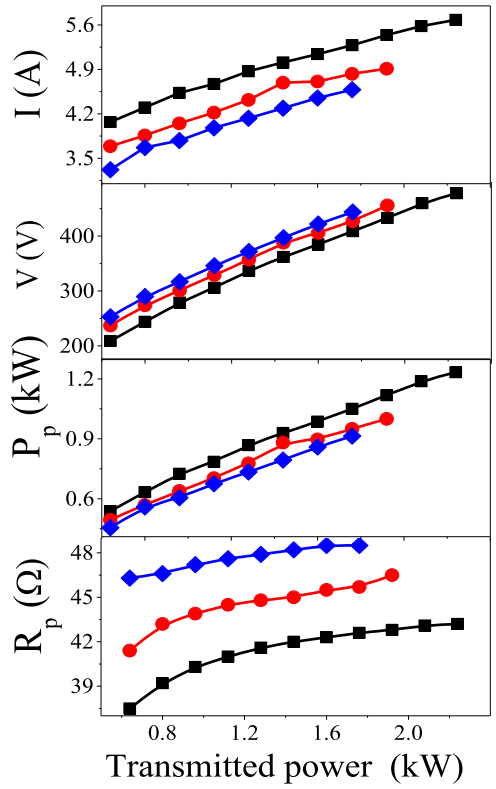

Figure 6. The dependence of the antenna rms current I, rms voltage V, power delivered to the plasma P_p, and the plasma resistance R_p, transformed to the antenna, on the input power for different Ar gas pressures: 1.3 Pa (squares), 2.6 Pa (circles), and 6.5 Pa (diamonds).

waveforms of the antenna input voltage and current, obtained with an Ar pressure of 6.5 Pa and 750 W of the power delivered to the plasma, P_p (see equation (1)), are shown in figure 5.

In figure 5(a), one can see a current spike corresponding to the gas breakdown and transition to the inductive mode of the discharge. Then, after about 150 ms, the antenna current reaches a steady state value. Such a long transition process (which is much longer than the plasma diffusion time) is due to the relatively long relaxation time of the RF generator self-adjustment feature. In addition, the plasma formation leads to a phase shift $\Delta\phi \approx 60°$ ($\cos\Delta\phi \approx 0.5$) between the voltage and current waveforms (figure 5(b)).

The measured root-mean-square (rms) values of the antenna current, I_a, and voltage, V_a, and the values of the power absorbed by plasma P_p and the corresponding plasma resistance R_p transformed to the antenna, calculated according to equation (1), are presented in figure 6 as functions of the transmitted power P_t. Having evaluated the plasma resistance R_p, one can calculate the ICP power transfer efficiency, $\eta = P_p/P_t = R_p/(R_p + R_0) = (1 + R_p/R_0)^{-1}$. Calculated this way, the ICP efficiency for the conditions presented in figure 6 is approximately 90%.

3.2. Plasma parameters

The Langmuir probe measurements showed that the plasma potential referenced to ground, V_p, was around 20 V. This value changed insignificantly for other pressures of Ar and He gas, as well as versus the RF power. Typical probe electrical characteristics, namely, the current density and its first and second derivatives versus the probe voltage referenced to the plasma potential and the calculated EEPF are shown in figure 7. Under the same experimental conditions, i.e. the pressure, gas type, and RF power, the reproducibility of the measured EEPF was ±5%.

An important aspect of wake field research is the axial and radial uniformity of the plasma density. Therefore, the Langmuir probe was used to obtain the axial and radial distributions of the plasma parameters in the chamber. The experimental results for the axial distributions are summarized in figures 8 and 9 for different gas pressures and RF powers delivered to the plasma.

One can see that the Ar plasma is relatively uniform along ~60 cm and that the plasma electron density is controllable in the range 10^{11}–10^{12} cm^{-3}. The electron temperature is also almost constant along the chamber and its value $\leqslant$3.5 eV. An increase in RF power leads to an increase in plasma density and a small decrease in electron temperature (see figures 8–10). This is typical for ICP gas discharge plasma, independently of the manner in which the plasma is generated [23]. Namely, the obtained small (~20%) decrease in the value of T_e with the ~3.5 times increase in power is related to possible two-step ionization and Maxwellization of the EEDF due to rising electron–electron collisions because of increased plasma electron density allowing the required ionization rate.

The radial distributions of the plasma electron density at $z = 45$ (middle of the chamber) for different Ar gas pressures and RF power are shown in figure 11. One can see that the plasma density is almost uniform within the column having a diameter of ~15 cm at a pressure <2.6 Pa and power <730 W.

The possible explanations of the obtained rather uniform axial and radial distributions of the plasma density can be related to the plasma particles transport governed by the charge exchange collisions (nonlinear transport) studied in details by Godyak [33] and Fruchtman, *et al* [34]. Non-uniform radial temperature distribution leading to depletion of the neutral density at the axis also can contribute to the obtained plasma density radial uniformity [35].

The parameters of the plasma were studied also in He ICP. The results of axial and radial distributions of He plasma density as compared to those of Ar plasma are presented in figure 12 for the lowest values of gas pressure, when rather uniform distributions were obtained. One can see that qualitatively the axial and radial distributions of the plasma density in the case of Ar and He plasmas are similar. However, for He plasma the electron density is about four times smaller than for Ar plasma at the same RF power delivered to the plasma. This difference is due to the difference in the ion mass and in the ionization potential for these gases. Note that the plasma loss on the walls is proportional to the ion sound speed $v_z = (T_e/M)^{1/2}$. A lower plasma density in He discharge is more suitable for wake field studies, because the maximum of the density modulations can be obtained when the plasma wavelength $\lambda_p = 2\pi/\omega_p \approx L \cong ct_{mw}$, where L is the length

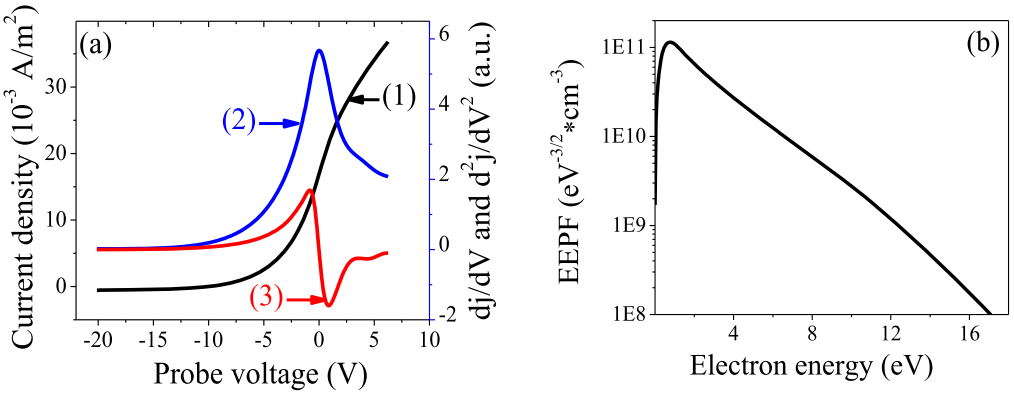

Figure 7. (a) Typical Langmuir probe current density (1), its first derivative (2), and its second derivative (3) for Ar pressure of 0.8 Pa; (b) electron energy probability function for Ar pressure of 0.8 Pa, $n_e = 5 \times 10^{11}$ cm^{-3}, $T_e = 2.3$ eV. The power delivered to the plasma was 900 W.

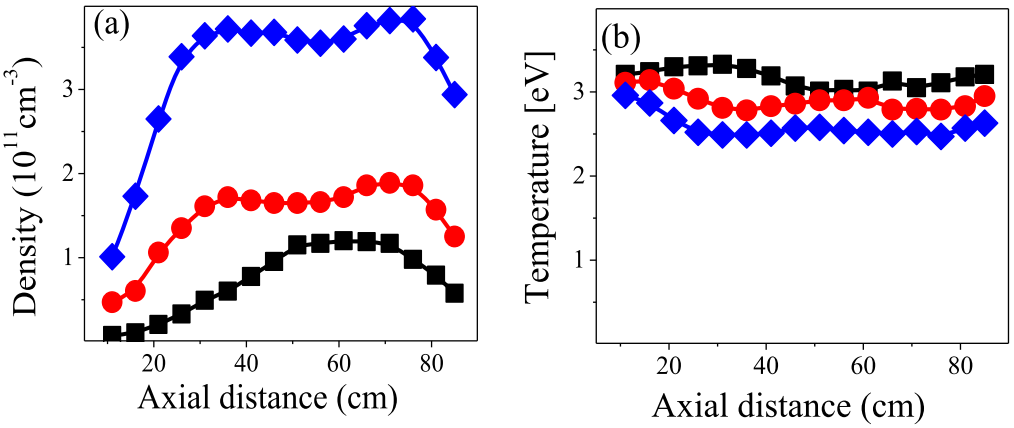

Figure 8. Axial distribution of the plasma density (a) and plasma electron temperature (b) at constant pressure of 0.8 Pa and different plasma powers of 340 W (squares), 660 W (circles), and 1200 W (diamonds).

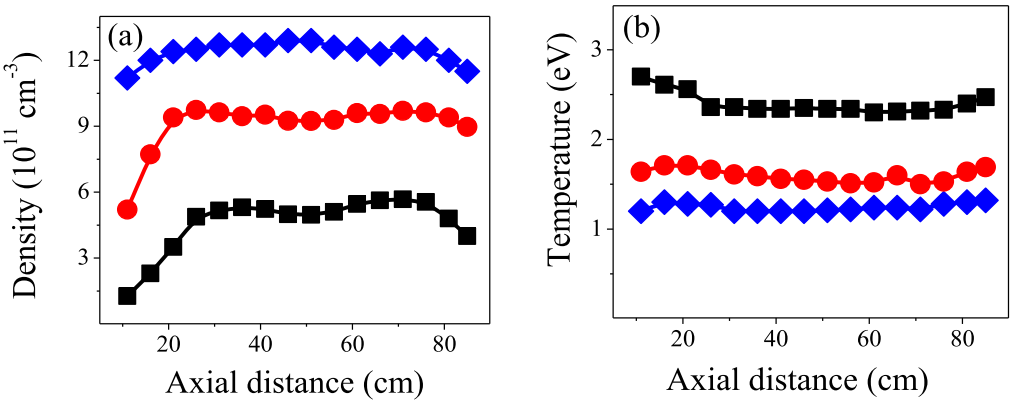

Figure 9. Axial distribution of the plasma density (a) and plasma electron temperature (b) at constant plasma power $P_p \cong 900$ W, and different Ar gas pressures of 0.8 Pa (squares), 2.6 Pa (circles), and 6.5 Pa (diamonds).

of the microwave beam, t_{mw} is its duration, and c is the speed of light [36]. For a microwave pulse duration of 0.5 ns, the plasma density should be $\leqslant 5 \times 10^{10}$ cm^{-3}.

To obtain an independent measurement of the plasma parameters, the microwave cut-off and microwave interferometry methods were applied to this ICP. For the cut-off measurements, the frequency of the CW microwave beam was changed between RF pulses, until a full cut-off of microwaves was observed. These experiments were conducted for ICP generated at three Ar gas pressures and RF powers and the results obtained were compared with simultaneous measurements of the plasma electron density by the Langmuir probe.

Typical waveforms of the detected microwave signal in the cases of full microwave cut-off and partial transmission measured by the receiving antenna are shown in figure 13.

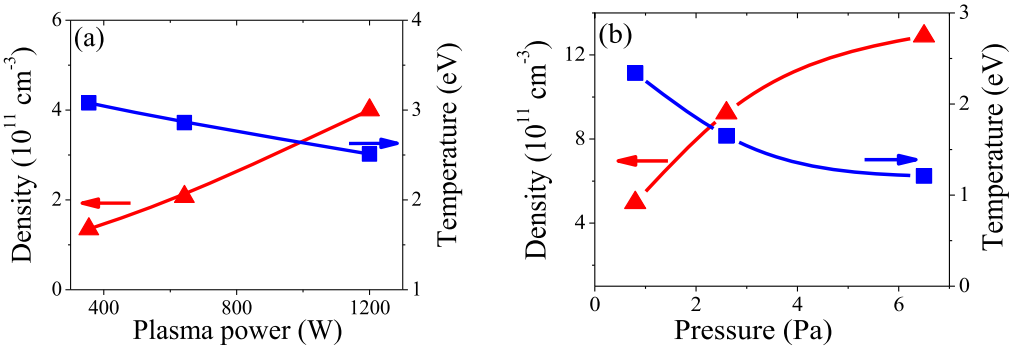

Figure 10. Plasma electron density and temperature at the axis of the plasma column in Ar discharge at the middle of the chamber for (a) different powers delivered to the plasma at Ar gas pressure of 0.8 Pa, (b) different Ar gas pressures at a constant plasma power $P_p \cong 900$ W.

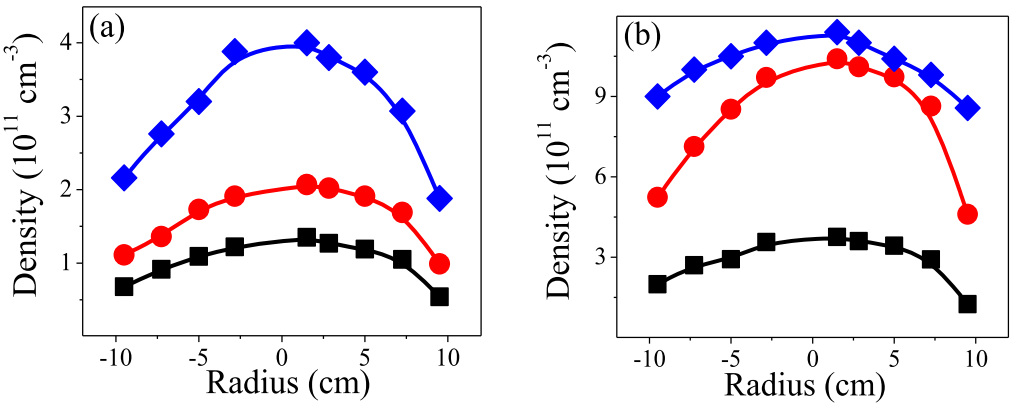

Figure 11. (a) Radial distribution of plasma density at constant pressure of 2.6 Pa and plasma power of 360 W (squares), 640 W (circles), and 1200 W (diamonds). (b) Radial distribution of plasma density for constant plasma power of 900 W and pressures of 0.8 Pa (squares), 2.6 Pa (circles), and 6.5 Pa (diamonds).

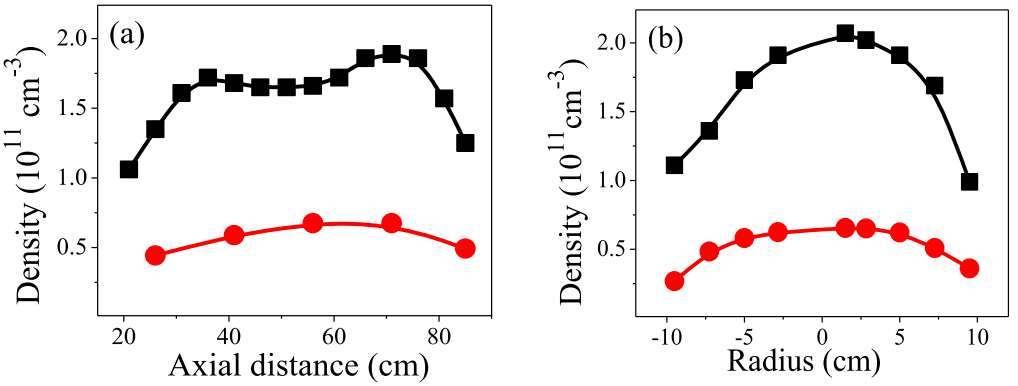

Figure 12. Axial (a) and radial (b) profiles of the plasma density in Ar (squares) and He (circles), at the lowest operating pressures (0.8 Pa and 1 Pa, respectively), at $P_p = 600$ W.

The obtained plasma electron density data for different gas pressures and RF power delivered to the plasma are presented in table 1. One can see a good agreement between the densities measured by the Langmuir probe and by the microwave cut-off method.

A typical waveform of the voltage, measured at the interferometer mixer output, obtained for an Ar pressure of 6.5 Pa and power delivered to the plasma of 750 W, is shown in figure 14. The phase shift is determined by adding $N_m \times \pi/2$ to the phase shift, where N_m is the number of maxima/minima or zero-crossings. The residual phase shift is determined by the ratio of the signal value at the steady state V_{steady} (the value of the mixed microwave signal when the plasma density does not change) to a known value at the maxima V_{max}, and the total phase shift is given by:

$$\Delta\phi = (N_m)\frac{\pi}{2} + \arcsin\left(\frac{V_{steady}}{V_{max}}\right). \quad (7)$$

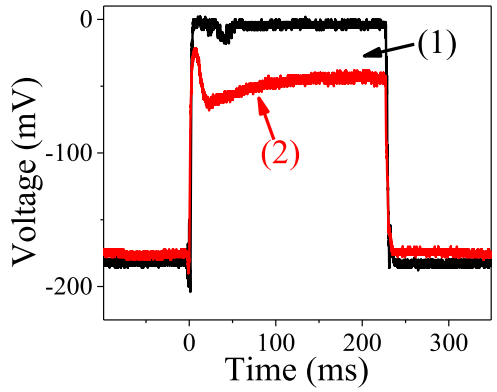

Figure 13. Typical waveform of the microwave power in the case of full cut off (1) $f = 10$ GHz, and partial transmission (2) $f = 15$ GHz, for Ar gas pressure of 4.0 Pa and plasma power of 560 W.

In our experimental conditions, the noise to signal ratio was about 5%. Applying equation (6), the resolution in the determination of the plasma density by the phase shift measurement was $\sim 5 \times 10^9\,\mathrm{cm}^{-3}$. At the first few ms after plasma ignition, the noise of the interferometer signal makes fringe counting problematic. Therefore, the absolute electron density was obtained using the afterglow region, where the signal was significantly less noisy. For the given example, the plasma electron density was determined to be $2.5 \times 10^{12}\,\mathrm{cm}^{-3}$. In addition, the interferometer data showed that the plasma density reached its steady state at ~150 ms with respect to the beginning of the RF discharge. During that time, the measured phase shift increases by 2π, which corresponds to a change in density of $6 \times 10^{11}\,\mathrm{cm}^{-3}$. The latter is ~20% of the density of the plasma at steady state conditions. This gradual increase in the plasma density matches the increase in the antenna current during the same time (see figure 5).

The results of the experiments using the interferometer are summarized in figure 15 for both Ar and He plasma. One can see a linear increase in the electron density with the power delivered to the plasma. These data are in satisfactorily good agreement with the results obtained using the Langmuir probe and microwave cut-off measurements for the same experimental conditions (see table 1).

OES also allows one to obtain averaged in sight of view parameters of the plasma and this method can be used to obtain the changes in the plasma density in the interaction region with the microwave drive. In these experiments, a gas mixture of 95% Ar/5% H_2 at a pressure of 1.3 Pa was used for ICP generation at a delivered RF power of 800 W, allowing the Balmer hydrogen lines to be observed and analyzed. In these experiments, simultaneously with OES, microwave interferometry was conducted during the same shots; it showed a plasma electron density of $2 \times 10^{11}\,\mathrm{cm}^{-3}$. Spectral line profiles were measured for H_α, H_β, and H_γ Balmer lines. As an example, the H_α line profile is shown in figure 16 with a Gaussian fit of this line:

$$I = I_0 \exp\left(\frac{(\lambda - \lambda_0)^2}{\sigma^2}\right), \tag{8}$$

where λ_0 is the central wavelength and $\sigma^2 = {\sigma_{\mathrm{line}}}^2 + {\sigma_{\mathrm{inst}}}^2$ is the line width, which is composed of the spectral line width and the instrumental width (here, the natural width of the spectral line is neglected).

In the present experimental conditions, the line width is dominated by the Doppler broadening, and thus, the gas temperature is measured [37]:

$$T\,[\mathrm{eV}] \approx 1.7 \times 10^8 \left(\frac{\Delta\lambda_{\mathrm{D\_FWHM}}}{\lambda_0}\right)^2 = 1.7 \times 10^8 \left(\frac{2\sigma_{\mathrm{line}}\sqrt{\ln(2)}}{\lambda_0}\right)^2. \tag{9}$$

The gas temperature, for these measurements, was found to be $T = 0.19$ eV, which is much lower than the plasma electron temperature. The latter can be explained by the long energy relaxation times between electrons and atoms, with density n and mass M [37]:

$$\tau_{\mathrm{kin}} \approx \left[7.5 \times 10^{-7}\left(\frac{13.6(\mathrm{eV})}{T_{\mathrm{e}}\,(\mathrm{eV})}\right)^{3/2}\right]^{-1} \frac{nM}{{n_{\mathrm{e}}}^2 m_{\mathrm{e}}}. \tag{10}$$

For the present experimental conditions, the relaxation time of electrons with H and Ar atoms exceeds 1 s, i.e., this time is much longer that the lifetime of atoms in an experimental chamber, which does not exceed 10 ms. Thus, the temperature of the neutrals and ions is significantly lower than that of the plasma electrons.

Electron temperature can also be measured using the line ratios of Balmer hydrogen lines. However, in the present experimental conditions, partial LTE cannot be considered either, and therefore, a CR model must be used to calculate the populations of energy levels. Since the lifetime of an atom in the Pyrex tube does not exceed 10 ms, time-dependent (TD) CR modeling [32] of the energy levels population was performed. The calculated population ratios of $n = 4$ to $n = 3$ and $n = 5$ to $n = 4$ levels in hydrogen, for $n_{\mathrm{e}} = 2 \times 10^{11}\,\mathrm{cm}^{-3}$ and different electron temperatures, are shown in figure 17. The experimental ratios, obtained from the Balmer series line ratios, were found to be 0.83 ± 0.02 for $n = 4$ to $n = 3$ level and 0.75 ± 0.02 for $n = 5$ to $n = 4$ level, which agrees with the modeling results for $T_{\mathrm{e}} = 1.4$ eV. This temperature is slightly lower than the electron temperature of 2.2 eV measured for ICP in the case of Ar gas by the Langmuir probe under the same input conditions (gas pressure and RF power delivered to the plasma). The latter can be related to the insertion of H_2 molecular gas, which can lead to a decrease in the electron temperature because of electron collisions with H_2 molecules.

For the case of electron temperature measurement in He plasma, for the described experimental conditions, a TD CR model must also be considered. Table 2 summarizes the line ratios, measured for a discharge with a background pressure of 6.5 Pa, 900 W power delivered to the plasma, and an electron density of $2 \times 10^{11}\,\mathrm{cm}^{-3}$.

The ratios of the spectral line intensities obtained for electron transitions $n = 4$ to $n = 2$ (numerator) and between the levels $n = 3$ and $n = 2$ (denominator) were chosen in

Table 1. Comparison of cut-off and Langmuir probe (LP) data.

Pressure (Pa)	Input power (W)	Electron density (LP) ($\times 10^{11}$ cm^{-3})	Cut-off frequency (GHz)	Electron density (cut-off) ($\times 10^{11}$ cm^{-3})	Electron density (interferometer) ($\times 10^{11}$ cm^{-3})
0.8	650	2.2	3.8	1.8	—
2.6	650	8.2	8.4	8.75	8.9
2.6	1100	11.1	10.7	14.2	14.5

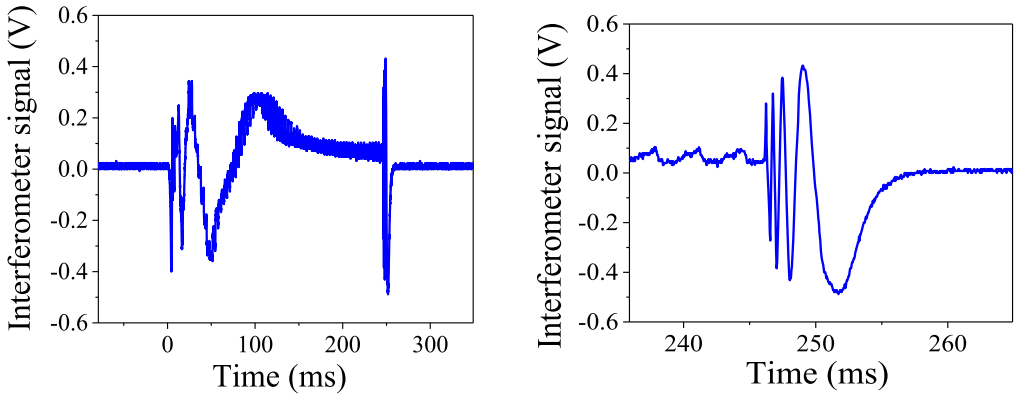

Figure 14. (a) A typical voltage waveform, obtained at the output interferometer mixer, during plasma operation; (b) zoom of the afterglow region. Conditions are the same as in figure 5. Plasma electron density obtained by the interferometer was 2.5×10^{12} cm^{-3}.

order to increase the energy difference between the upper excited states. The electron temperature, analyzed by the Langmuir probe for the same conditions, was found to be ~3 eV. However, the results of the TD CR modeling for the measured plasma density and the atom lifetime in the system (<15 ms) showed no match to the measured ratio. For example, for $T_e = 3$ eV, the model ratios of 447.1/587.6 nm, 471.3/501.6 nm, and 492.2/667.8 nm are 0.15, 21, and 0.12, respectively. These deviations from the experimental results were found also for all ranges of expected plasma electron temperatures and densities. However, introducing a small portion of 'hot' electrons in the CR modeling (a Maxwellian distribution with a higher electron temperature) improves agreement between modeling and measurements. For example, adding 5% high energy electrons with a temperature of 70 eV changes the ratios to 0.17, 0.98, and 0.27, respectively. The best match with the experimental results was found for CR modeling that considers 95% of plasma electrons with $T_e \sim 1$ eV and ~5% of electrons with $T_e \sim 70$ eV, which results in ratios of 0.21, 0.55, and 0.3, respectively. Here, let us note that the ratios obtained by the model are sensitive to the distribution function and energy of the 'hot' electrons. Nevertheless, these data strongly indicate that a small part of the plasma electrons have an energy that significantly exceeds the thermal energy of the main part of the plasma electrons.

4. Discussion

Carried out experiments showed reliable formation of a rather uniform and meter-scale plasma with controllable density in the range (5×10^{10}–10^{12} cm^{-3}). For experiments with wake-field formation, however, the density $<5 \times 10^{10}$ cm^{-3} is required in order to obtain significant (>20%) plasma density modulations. Thus, these experiments will be performed either with He plasma allowing smaller plasma density while keeping it radial and axial uniformity, or with decreased plasma density due to its decay. In the latter case, wake field experiments will be carried out with some controllable time delay with respect to the termination of the RF pulse.

Using the measured density and temperature of the plasma electrons, the parameters of the RF discharge plasma for known gas pressures can be analyzed. The frequency of elastic collisions of electrons with neutral atoms can be roughly estimated as [14]:

$$\nu_m = n_g \langle \sigma_{el} v_{th} \rangle, \tag{11}$$

where n_g is the gas density, $\sigma_{el} \approx 10^{-15}$ cm^2 is the elastic cross section and $v_{th} = \sqrt{(8kT_e)/(\pi m_e)}$ is the thermal velocity of the electron having Maxwellian energy distribution. For a dissipated power of 900 W, the experimental data show (see figure 9(b)) that for gas pressures in the range 0.8–6.5 Pa, the measured value of T_e decreases in the range 2.5–1.2 eV. For these plasma parameters, the electron elastic collision frequency changes in the range (0.85–2.2) $\times$ 10^7 s^{-1} [38]. This range of frequency is comparable with the ICP driving frequency $\omega = 1.25 \times 10^7$ s^{-1} and the skin-depth transient frequency $\omega_{th} = v_{th}/\delta \approx 5 \times 10^7$ s^{-1}, and is significantly smaller than the plasma frequency $\omega_p = 6 \times 10^9 - 6 \times 10^{10}$ s^{-1}. In these conditions, the RF discharge has features of collisional δ_c and anomalous δ_e skin effect, for which the skin depth is defined as [39]:

$$\delta_c = \frac{c}{\omega_p}\left(\frac{2\nu_m}{\omega}\right)^{1/2}, \tag{12}$$

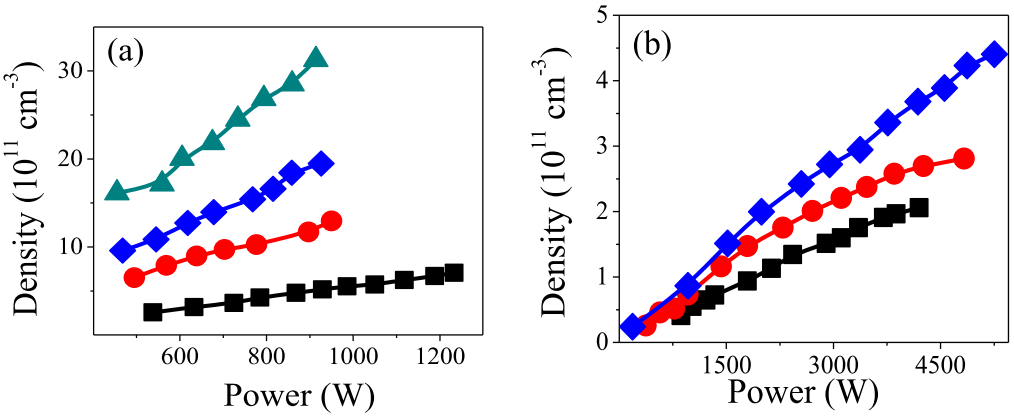

Figure 15. Plasma electron density, measured by the interferometer, versus the RF power delivered to the plasma for (a) Ar gas at pressures of 1.3 Pa (squares), 2.6 Pa (circles), 4.0 Pa (diamonds), and 6.5 Pa (triangles). (b) He gas at pressures of 2.6 Pa (squares), 6.5 Pa (circles) and 13 Pa (diamonds).

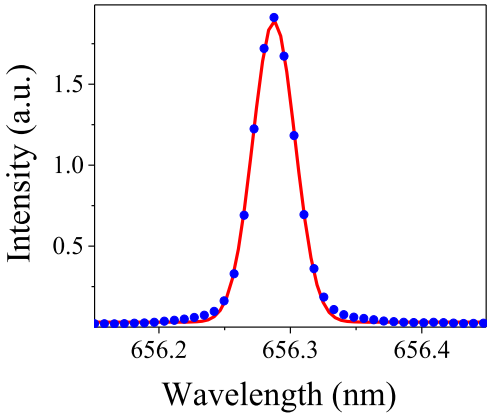

Figure 16. Profile of H_α spectral line (dots) and Gaussian fit of the line shape (line).

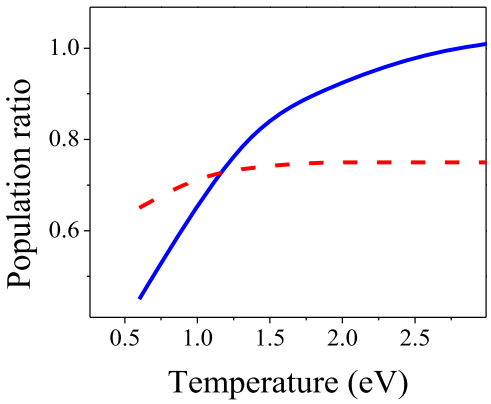

Figure 17. Dependence of population ratios of hydrogen atom energy levels, $n = 4$ to $n = 3$ (solid line) and $n = 5$ to $n = 4$ (dashed line), obtained by CR modeling versus electron temperature for electron density of 2×10^{11} cm^{-3}.

Table 2. Helium spectral line ratios for $p = 6.5$ Pa, $P_p = 900$ W, and $n_e = 2 \times 10^{11}$ cm^{-3}.

Spectral lines (nm)	447.1/587.6	471.3/501.6	492.2/667.8
Measured ratio (Photons/s AU)	0.24 ± 0.01	0.50 ± 0.02	0.26 ± 0.01

$$\delta_e = (cv_{th}{}^2/2\omega\omega_p{}^2)^{1/3}. \quad (13)$$

The estimated values of the skin depths according to equations (12) and (13) are close to each other and are in the range 1.5–2.5 cm, which is significantly smaller than the distance (~20 cm) between the arms of the quadruple antenna. Therefore, the main RF energy deposition into the plasma occurs near the antenna wires. It should be mentioned that the expressions above for the skin depth are derived for uniform semi-infinite plasma with a planar boundary. In practical ICP, and in particular for the quadruple antenna that was used, the real electromagnetic field distribution in the skin layer is affected by the geometric skin depth occurring even without plasma because of the field curvature [40]. Therefore, the real skin depth would be smaller than the values estimated above.

In general, the spatial distributions of the bounded plasma parameters are defined by the size of the plasma, gas pressure, and heating field profile. Under the conditions of our experiments with ICP at low gas pressure, the electron energy relaxation length λ_ε for the majority of plasma electrons (having energy ε lower than the excitation energy $\varepsilon^* = 11.5$ eV) exceeds the plasma radius, $\lambda_\varepsilon \approx \lambda_{el}(M_{Ar}/2m_e)^{1/2} > R$. Here, λ_{el} is the electron elastic mean free path length, M_{Ar} is the Ar atom mass, and R is the radius of the plasma column. Under these conditions, known as the domain of non-local electron kinetics [41], the plasma electrons behave as a gas with infinite thermo-conductivity, $\nabla T_e \approx 0$, and the plasma parameters are not local functions of the electric heating field; thus, $T_e(r)$ and $n_e(r)$ are practically independent of the spatial distribution of the RF field $E_{rf}(r)$. Under our experimental conditions, the assumption of non-local electron kinetics is well satisfied (in both the radial and axial directions) for low energy electrons with $\varepsilon < \varepsilon^*$. The condition of nonlocal electron kinetics is not satisfied for electrons in the inelastic energy range ($\varepsilon > \varepsilon^*$), which results in some local features for the excitation and ionization processes leading to localization within the skin layer. The consequence of this partial locality is that the ionization rate along the antenna wires is equalized and the enhanced ionization on the plasma axial ends, thus, flattening the

plasma density axial distribution. The azimuthal part of the antenna coil located at its end also contributes to ionization enhancement at the plasma axial ends. Note that without these local effects, the axial plasma distribution is expected to be cosine-like.

The plasma density radial distribution is defined by the ratio of the ion mean free path λ_i to the plasma column radius $R = 12$ cm. The value of λ_i can be estimated as $1/\sigma_{in} n_g$, where σ_{in} is the cross section for ion-neutral collision, which for ions in ambipolar motion is controlled by the charge exchange with neutrals [31]. For ion energy $T_i \approx 1$eV, in ambipolar radial motion, at $p = 2.6$ Pa, one obtains $\lambda_i \approx 0.16$ cm, which is smaller than $T_g/T_e R$. Here, T_g is the gas temperature. In such conditions, the plasma bulk radial density distribution can be well described by the classical diffusional model which assumes that the ion inertia and ionization terms are significantly smaller than the ion friction term [42]:

$$n(r) \approx n_0 J_0\left(\frac{2.405}{R} r\right), \tag{14}$$

where n_0 is the density at the axis and J_0 is the Bessel function. Here, let us note that $r = 10$ cm, where the plasma density was measured (see figure 11) and $n(r) \approx 0.5 n_0$, which is ~2 times larger than the expected value of the density according to equation (14). However, let us note that, due to partial locality, the plasma density in the skin area near the antenna wires can be somewhat larger than that given by equation (14).

Now let us estimate the plasma resistivity. The electron–ion collision frequency inside the skin layer can be estimated as [31]:

$$\nu_{ei} = n_e v_{th} \sigma_{col} = n_e v_{th} \frac{4\pi}{9} \frac{e^4 \ln \Lambda}{(kT_e)^2}, \tag{15}$$

where σ_{col} is the Coulomb cross section and $\ln \Lambda$ is the Coulomb logarithm. For the present experimental conditions, the electron–ion collision frequency is $<10^6\ s^{-1}$. This is lower by more than an order of magnitude than the electron–neutral collision frequency and therefore in these estimates of the plasma resistivity electron–ion collisions will be neglected. Because $\nu_m > \nu_{ei}, \nu_{eff}$, the resistivity of the plasma can be estimated as [14]:

$$\rho_p \approx \frac{m\nu_m}{e^2 n_e}. \tag{16}$$

These estimates show that for the entire range of the experimental conditions in the case of Ar gas discharge, the resistivity of the plasma is around $3 \times 10^{-2}\ \Omega$ m.

Next, by using the estimated resistivity, it is possible to obtain the rms current density in the plasma, considering that the major part of the current is limited to inside the area with a radius equal to the skin depth δ_c, and taking into account that the plasma density at a distance ~1 cm from the wall is $n(r = 11\text{ cm}) \approx 0.1 n_0$:

$$\langle J \rangle = 0.5\left(\frac{P_p}{S_i l \rho_p}\right)^{1/2}, \tag{17}$$

where $S_i \approx 9\ cm^2$ is the cross section of the current carrying area inside the plasma, taking into account the wires located at a single arm of the antenna, $P_p = 900$ W is the total power delivered to the plasma, and $l = 0.8$ m is the length of the antenna. In this rough estimation, most of the RF power delivered to the plasma was considered to be absorbed uniformly in the plasma semi-column with the calculated skin depth along the antenna, and edge effects were ignored.

Applying the parameters for Ar plasma, with $P_p = 900$ W, under conditions similar to those presented in figure 9, the current density in the plasma is $\sim 0.1\ A\ cm^{-2}$. In addition, with these assumptions, and also neglecting the capacitive coupling, one obtains the integral of the electric field along the plasma:

$$\langle V_P \rangle = \langle E \rangle l = \rho_p \langle J \rangle l. \tag{18}$$

which is estimated as ~24 V, resulting in an rms axial electric field of only $\sim 30\ V\ m^{-1}$.

5. Summary

A plasma source system designed for microwave wake-field experiments was investigated and characterized. This system allows uniform, meter-scale plasma with a wide range of densities (10^{10}–$10^{12}\ cm^{-3}$) and electron temperature 1–5 eV to be generated. To study the plasma parameters, four independent methods of plasma diagnostics (Langmuir probe, microwave interferometry, microwave cut-off, and optical spectroscopy) were applied and the plasma densities obtained by these methods were found to be in good agreement. The plasma is generated by a quadruple antenna transmitting RF power to the plasma in a cm-size skin layer. The long energy relaxation length of electrons allows almost constant axial and radial distribution of electron temperature in the plasma bulk. The application of the quadruple antenna with resonating capacitors inserted in its arms decreases the stray antenna capacitance and capacitive coupling to the plasma, resulting in a reduction of the plasma RF potential and the RF power loss in the antenna. Such a design allows the generation of scalable, rather uniform plasma along the axial direction of the system with a well-defined radial profile. These features make the developed plasma source suitable for microwave plasma wake-field experiments.

Acknowledgments

The authors are grateful to A Fisher and Y Hadas for fruitful discussions and E Flyat for generous technical assistance. This work was supported by the PAZY grant No 2020960. The work of Denis Zolotukhin was supported by the Russian Foundation for Basic Research (RFBR), grant No 16-38-00230. The work Valery Godyak was supported in part by the DOE OFES (Contract No DE-SC0001939).

References

[1] Tajima T and Dawson J 1979 Laser electron accelerator *Phys. Rev. Lett.* **4** 267–70

[2] Leemans W P, Nagler B, Gonsalves A J, Tóth C, Nakamura K, Geddes C G R, Esarey E, Schroeder C B and Hooker S M 2006 GeV electron beams from a centimetre-scale accelerator *Nat. Phys.* **2** 696–9

[3] Malka V 2012 Laser plasma accelerators *Phys. Plasmas* **19** 55501

[4] Chen F F 1996 Physics of helicon discharges *Phys. Plasmas* **3** 1783

[5] Sudit I D and Chen F F 1999 Discharge equilibrium of a helicon plasma *Plasma Sources Sci. Technol.* **5** 43–53

[6] Windisch T, Rahbarnia K, Grulke O and Klinger T 2010 Study of a scalable large-area radio-frequency helicon plasma source *Plasma Sources Sci. Technol.* **19** 55002

[7] Shinohara S and Tanikawa T 2005 Characteristics of a large volume, helicon plasma source *Phys. Plasmas* **12** 44502

[8] Shinohara S and Tanikawa T 2004 Development of very large helicon plasma source *Rev. Sci. Instrum.* **75** 1941–6

[9] Holkundkar A, Brodin G and Marklund M 2011 Wakefield generation in magnetized plasmas *Phys. Rev.* E **84** 36409

[10] Leonhardt D, Walton S G, Blackwell D D, Amatucci W E, Murphy D P, Fernsler R F and Meger R A 2001 Plasma diagnostics in large area plasma processing system *J. Vac. Sci. Technol.* A **19** 1367

[11] Rosenman G, Shur D, Krasik Y E and Dunaevsky A 2000 Electron emission from ferroelectrics *J. Appl. Phys.* **88** 6109

[12] Gilson E P, Davidson R C, Efthimion P C, Gleizer J Z, Kaganovich I D and Krasik Y E 2012 Plasma source development for the NDCX-I and NDCX-II neutralized drift compression experiments *Laser Part. Beams* **30** 435–43

[13] Conrads H and Schmidt M 2000 Plasma generation and plasma sources *Plasma Sources Sci. Technol.* **9** 441–54

[14] Chabert P and Braithwaite N 2011 *Physics of Radio-Frequency Plasmas* (Cambridge: Cambridge University Press)

[15] Godyak V A, Piejak R B and Alexandrovich B M 1991 Electrical characteristics of parallel-plate RF discharges in argon *IEEE Trans. Plasma Sci.* **19** 660–76

[16] Perrin J, Schmitt J, Hollenstein C, Howling A and Sansonnens L 2000 The physics of plasma-enhanced chemical vapour deposition for large-area coating: industrial application to flat panel displays and solar cells *Plasma Phys. Control. Fusion* **42** B353–63

[17] Setsuhara Y, Ono K and EBE A 2007 Development of a meters-scale large area plasma reactor using multiple low-inductance antenna modules for giant electronics processing *Trans. JWRI* **36** 95–7

[18] Godyak V A, Piejak R B and Alexandrovich B M 1991 Ion flux and ion power losses at the electrode sheaths in a symmetrical RF discharge *J. Appl. Phys.* **69** 3455–60

[19] Godyak V A and Piejak R B 1990 Probe measurements of the space potential in a radio frequency discharge *J. Appl. Phys.* **68** 3157–62

[20] Godyak V A, Piejak R B and Alexandrovich B M 1999 Experimental setup and electrical characteristics of an inductively coupled plasma *J. Appl. Phys.* **85** 703

[21] Kral'kina E A 2008 Low-pressure radio-frequency inductive discharge and possibilities of optimizing inductive plasma sources *Phys.—Usp.* **51** 493–512

[22] Kim S S, Chang H Y, Chang C S and Yoon N S 2000 Antenna configuration for uniform large-area inductively coupled plasma production *Appl. Phys. Lett.* **77** 492–4

[23] Godyak V A, Piejak R B and Alexandrovich B M 2002 Electron energy distribution function measurements and plasma parameters in inductively coupled argon plasma *Plasma Sources Sci. Technol.* **11** 525–43

[24] Godyak V A and Demidov V I 2011 Probe measurements of electron-energy distributions in plasmas: what can we measure and how can we achieve reliable results ? *J. Phys. D: Appl. Phys.* **44** 233001

[25] Godyak V A and Alexandrovich B M 2015 Comparative analyses of plasma probe diagnostics techniques *J. Appl. Phys.* **118** 233302

[26] Kim J H, Seong D J, Lim J Y and Chung K H 2003 Plasma frequency measurements for absolute plasma density by means of wave cutoff method *Appl. Phys. Lett.* **83** 4725–7

[27] Hutchinson I H 2002 *Principles of Plasma Diagnostics* (Cambridge: Cambridge University Press)

[28] Andrasch M, Ehlbeck J, Foest R and Weltmann K-D 2012 Electron density measurements on an inductively coupled plasma with a one-port microwave interferometer *Plasma Sources Sci. Technol.* **21** 55032

[29] Iordanova S and Koleva I 2007 Optical emission spectroscopy diagnostics of inductively driven plasmas in argon gas at low pressures *Spectrochim. Acta* B **62** 344–56

[30] Godyak V A www.plasmasensors.com/articles/ProbeDiagnosticsTutorial.pdf

[31] Raizer Y P 1991 *Gas Discharge Physics* ed J E Allen (Berlin: Springer)

[32] Ralchenko Y V and Maron Y 2001 Accelerated recombination due to resonant deexcitation of metastable states *J. Quant. Spectrosc. Radiat. Transf.* **71** 609–21

[33] Godyak V A 1990 Non-local bounded plasma model with charge exchange collisions *ESCAMPIG-90, Contributed Papers* ed B Dubreuil (Orleans, France: European Physical Society) pp 415–22

[34] Fruchtman A 2005 Two-dimensional equilibrium of a low temperature magnetized plasma *Plasma Sources Sci. Technol.* **14** 152–67

[35] Fruchtman A 2008 Energizing and depletion of neutrals by a collisional plasma *Plasma Sources Sci. Technol.* **17** 24016

[36] Esarey E, Schroeder C and Leemans W 2009 Physics of laser-driven plasma-based electron accelerators *Rev. Mod. Phys.* **81** 1229–85

[37] Griem H R 1997 *Principles of Plasma Spectroscopy* (Cambridge: Cambridge University Press)

[38] Lister G G, Li Y-M and Godyak V A 1996 Electrical conductivity in high-frequency plasmas *J. Appl. Phys.* **79** 8993

[39] Lieberman M A and Lichtenberg A J 2005 *Principles of Plasma Discharges and Materials Processing* 2nd edn (New York: Wiley)

[40] Godyak V A and Piejak R B 1997 Electromagnetic field structure in a weakly collisional inductively coupled plasma *J. Appl. Phys.* **82** 5944

[41] Kolobov V I and Godyak V A 1995 Nonlocal electron kinetics in collisional gas discharge plasmas *IEEE Trans. Plasma Sci.* **23** 503–31

[42] Godyak V A and N Sternberg N 2008 Two-dimensional cylindrical plasma at low gas pressure *Plasma Sources Sci. Technol.* **17** 25004